JPE 15-6-14

http://dx.doi.org/10.6113/JPE.2015.15.6.1547
ISSN(Print): 1598-2092 / ISSN(Online): 2093-4718

A High Performance Permanent Magnet Synchronous Motor Servo System Using Predictive Functional Control and Kalman Filter

Shuang Wang[†], Wenju Zhu[*], Jian Shi[*], Hua Ji[*], and Surong Huang[*]

[†*]School of Mechatronic Engineering and Automation, Shanghai University, Shanghai, China

Abstract

A predictive functional control (PFC) scheme for permanent magnet synchronous motor (PMSM) servo systems is proposed in this paper. The PFC-based method is first introduced in the control design of speed loop. Since the accuracy of the PFC model is influenced by external disturbances and speed detection quantization errors of the low distinguishability optical encoder in servo systems, it is noted that the standard PFC method does not achieve satisfactory results in the presence of strong disturbances. This paper adopted the Kalman filter to observe the load torque, the rotor position and the rotor angular velocity under the condition of a limited precision encoder. The observations are then fed back into PFC model to rebuild it when considering the influence of perturbation. Therefore, an improved PFC method, called the PFC+Kalman filter method, is presented, and a high performance PMSM servo system was achieved. The validity of the proposed controller was tested via experiments. Excellent results were obtained with respect to the speed trajectory tracking, stability, and disturbance rejection.

Key words: Predictive functional control, Kalman filter, Disturbance observer, Torque compensation, Permanent magnet synchronous motor

I. INTRODUCTION

During the past two decades, permanent magnet synchronous motors (PMSMs) have been generally replacing DC motors and induction motors in a great many industrial applications, such as electric vehicles, numerically controlled machine tools and robotics. It is able to offer numerous advantages over the two previously mentioned motors, including a simple structure, high efficiency, high power density and high torque-to-current ratio. Despite its advantages, it is still challenging to control a PMSM to achieve good transient performance under all operating conditions. This is due to the fact that PMSMs are multivariable, nonlinear and strong-coupled systems that are extremely sensitive to parameters and disturbances.

The traditional proportional integral (PI) control is usually used to adjust the static and dynamic performance of a system as a classical linear control scheme. However, the servo system of a PMSM makes it difficult to achieve a good control effect with the PI control scheme due to the presence of nonlinearity and uncertainty [1]. Scholars have put forward many advanced control methods to optimize the servo systems of PMSMs in recent years, e.g., model reference adaptive control [2], feedback linearization [3], fuzzy control [4], H_∞ control [5], sliding mode control [6], disturbance observer-based (DOB) control [7], [8], and neural network control [9], [10]. These approaches have been successfully applied to PMSM servo systems, and can improve different aspects of the control performance of a motor.

Predictive control is a computer control algorithm. It has an excellent control effect and is suitable for industrial production processes which are relatively complex and where it is difficult to establish an accurate digital model, because it uses a multi-step test, receding optimization and feedback correction strategy [11]. Model predictive control (MPC) is the most widely used method of predictive control. The core of the MPC is to replace a 'closed loop optimal control' with an 'open-loop optimal control' in a time-varying region. There are many research reports on the application of the MPC method to PMSM servo systems. The controllers developed in [3], [12] give good performance. However, the MPC

Manuscript received Jan. 1, 2015; accepted Jun. 18, 2015
Recommended for publication by Associate Editor Dong-Hee Lee.
[†]Corresponding Author: wang-shuang@shu.edu.cn
Tel: +86-136-0186-0669, Shanghai University
[*]School of Mechatronic Engineering and Automation, Shanghai University, China

control requires too many calculations, which makes this method difficult to apply to fast dynamic systems [13].

A simplified MPC method, i.e., the predictive functional control (PFC) method, is employed as the adopted control scheme in this study. This method was presented by Richalet et al. in 1993 [14]. PFC which enhances the advantages of this method, such as feed-forwarding, constraints handling, no-lag error on the dynamic set points, is an easy trade-off between robustness and dynamic specifications. It not only retains the advantages of on-line optimization and constraint processing of the MPC, but also has a lower online computational burden, which can achieve a simpler and more intuitive design criteria combined with a higher control precision [15].

In practical industrial applications, disturbances always exist. Standard PFC methods cannot reject them well. Because PFC assumes that all un-modeled signals remain the same with prediction current errors, which makes it hard to counteract steady-state errors when encountering interference or an inaccurate model, especially in the presence of strong interference conditions, which may cause deterioration of the performance of the closed-loop control, it is difficult for the prediction model to precisely predict future outputs [16]. As a result, the future control action obtained by optimizing a certain performance index cannot react well to resist disturbances. In [16], the scholars presented a combination control strategy made up of a PFC method with an extended state observer (ESO). This strategy can reduce prediction errors and improve the performance of the PFC. The above studies focused on external disturbance influences on a system. However, the quantization error of the speed feedback also influences the performance of PFC system.

The Kalman filter (KF) which is based on minimum variance, has been widely used in drive control areas as an estimator, because of its excellent performance under noisy conditions and its wide speed control range [17]. In [18], the control is achieved through nonlinear quadratic optimal control, and an extended Kalman filter is used for parametric estimation. In [19], it can be used for the estimation of the joint state and parameters as well as unknown disturbances in noisy environments. In [20], a Kalman filter is used to observe external disturbances. In [21], taking a Kalman filter as an observer, excellent results verified the performances of the observer. Based on this, an improved PFC method, called the PFC+Kalman filter method, is proposed in this paper. A Kalman filter is constructed to obtain information on the rotor position, speed and load torque. Then the PFC controller is compensated with the observed values, and the PFC model is reconstructed. Finally, the improved PFC method in this paper was verified by an experiment. The results verify its effectiveness in terms of speed detection and disturbance rejection.

This paper is organized as follows. In section II, the PMSM model is presented. Section III presents the design details of a speed controller using the PFC method. The studied PFC+Kalman filter is developed in Section IV for the speed loop. Section V gives implementation and experimental results of the predictive control scheme for the PMSM servo system. Section VI concludes the paper.

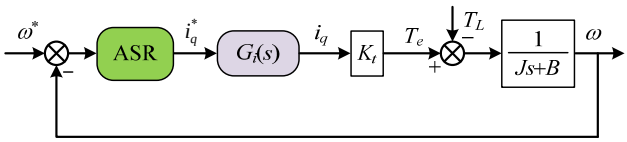

Fig. 1. Block diagram of the simplified PMSM control system.

II. Mathematical Model of a PMSM

The mathematical model of a surface mounted PMSM in the rotor reference frame can be expressed in the bilinear form as [11]:

$$\frac{d}{dt}\begin{bmatrix} i_d \\ i_q \\ \omega \end{bmatrix} = \begin{bmatrix} -R_s/L_a & n_p\omega & 0 \\ -n_p\omega & -R_s/L_a & n_p\psi_f/L_a \\ 0 & K_t/J & -B/J \end{bmatrix}\begin{bmatrix} i_d \\ i_q \\ \omega \end{bmatrix} + \begin{bmatrix} u_d/L_a \\ u_q/L_a \\ -T_L/J \end{bmatrix} \quad (1)$$

Where, u_d and u_q are the *d*-axis and *q*-axis components of the armature voltage, i_d and i_q are the *d*-axis and *q*-axis components of the armature current, R_s is the stator resistance, L_a is the stator inductance, L_d and L_q are the inductances of the *d*-*q* axes satisfying $L_d = L_q = L_a$, n_p is the number of pole pairs, ψ_f is the rotor of the permanent magnet flux linkage, ω is the rotor angular velocity, T_L is the motor load torque, J is the moment of inertia, and B is the coefficient of the friction.

The field oriented control (FOC) strategy is employed for PMSM. Under this scheme, the automatic speed regulator (ASR) and the automatic current regulator (ACR) are cascaded, and the d-axis reference current is usually set to be zero. Then, the electromagnetic torque is given as:

$$T_e = 1.5 n_p \psi_f i_q = K_t i_q \quad (2)$$

The implementation of the predictive functional control strategy depends on an appropriate model. The dynamic model of the motor is a nonlinear and strong coupling system, because the current band width is far greater than the speed loop bandwidth. If the PI parameter is tuning properly, the sampling of the current can be equal to the reference current, $i_q = i_q^*$. Then, the current loop transfer function is reduced to $G_i(s) = 1$. The simplified block diagram of a PMSM is shown in Fig. 1.

According to the Laplace transform, the mechanical equation of a dynamic model for a motor is:

$$\omega(s) = \frac{K_t i_q^*(s) - T_L(s)}{Js + B} \quad (3)$$

III. PFC CONTROLLER DESIGN FOR A PMSM

In practical applications, PFC restructures the control inputs by considering each moment of the control inputs as a linear combination of several pre-selected basic functions, and then obtaining a linear weighting coefficient through the online optimization, and finally getting the control input of the future [12]. In this paper, the PFC design process is as follows:

A. Base Functions

The controlled variable can be expressed as a linear combination of several known base functions in the PFC control strategy. It is related to the plant characteristic and the tracking set value.

$$u(k+i)=\sum_{j=1}^{N}\mu_j f_j(i) \tag{4}$$

Where, $u(k+i)$ is the system output at time $(k+i)$. The choice of base functions depends on the characteristics of the controlled plant and the set values, such as a step, ramp and exponential function. The desirable output control variable of the PFC is the reference current i_q^* [16].

Therefore:

$$i_q^*(k+i)=\sum_{j=1}^{N}\mu_j f_j(i) \tag{5}$$

Where, $f_j(i)$ is the value of the base functions at time $t=iT_S$, T_S is the sampling period, i=1,2,⋯h, h is the predictive optimal length, and μ_j is the linear combination coefficient. Because the choice of basic functions does not directly affect the stability or the dynamic state of a closed-loop system, this system chooses a step function as the base functions, Set $N=1$, $f_1(\mathrm{i})=1$.

Therefore:

$$i_q^*(k)=\mu_1 \tag{6}$$

B. Prediction Model

A prediction model is used to predict the output of a process in a future period of time according to historical information and the current input of objects studied. By considering the load $T_L(\mathrm{s})$, equation (3) can be written in the form of difference equation after zero-order holder discrete sampling:

$$\omega_m(k+1)=\alpha_m\omega_m(k)+K_m i_q^*(k)+K_m\hat{T}_L(k)/K_t \tag{7}$$

Where, $\alpha_m=e^{-T_S B/J}$ and $K_m=(1-\alpha_m)K_t/B$ are both the coefficients of a prediction model equation. $\omega_m(k+1)$ is the speed prediction value at time $(k+1)$. In the next sampling time $(k+2)$:

$$\begin{aligned}\omega_m(k+2)=\alpha_m\omega_m(k+1)+K_m i_q^*(k+1)\\ +K_m\hat{T}_L(k+1)/K_t\end{aligned} \tag{8}$$

According to the mean-level control method, assuming that the values of the control variables are a constant in the future, $i_q^*(k)=i_q^*(k+1)=\cdots=i_q^*(k+h-1)$. Substituting (7) into (8) yields:

$$\begin{aligned}\omega_m(k+2)=\alpha_m^2\omega_m(k)+K_m(1+\alpha_m)i_q^*(k)\\ +K_m(1+\alpha_m)\hat{T}_L(k)/K_t\end{aligned} \tag{9}$$

Followed by the superposition, the output of the prediction model can be obtained as:

$$\begin{aligned}\omega_m(k+i)=\alpha_m^i\omega_m(k)+K_m(1+\alpha_m+\cdots+\alpha_m^{i-1})i_q^*(k)\\ +K_m(1+\alpha_m+\cdots+\alpha_m^{i-1})\hat{T}_L(k)/K_t\end{aligned} \tag{10}$$

Equation (10) can be written in a matrix form as:

$$W_m(k)=W_o(k)+W_b(k)[\mu_1(k)+\hat{T}_L(k)/K_t] \tag{11}$$

Where:

$$W_m(k)_{(h\times1)}=[\omega_m(k+1)\cdots\omega_m(k+h)]^T$$

$$W_o(k)_{(h\times1)}=[\alpha_m\cdots\alpha_m^h]^T\omega_m(k)$$

$$W_b(k)_{(h\times1)}=[K_m\cdots K_{\mathrm{m}}(1+\cdots+\alpha_{\mathrm{m}}^{h-1})]^T$$

C. Error Correction

Considering model adaptation, parameter detuning and interference, the actual output and the predicted output usually contain some errors. System error during the prediction time domain can be considered to be the same as the error at this time.

$$e(k+i)=\cdots=e(k+1)=e(k)=\omega(k)-\omega_m(k) \tag{12}$$

Where, $\omega(k)$ is the practical system output measured at time k.

D. Reference Trajectory

For a stable system, a first-order exponential form is usually used. Accordingly, the reference trajectory equation is as follows:

$$\omega_r(k+i)=\omega^*(k+i)-\alpha_r^i[\omega^*(k)-\omega(k)] \tag{13}$$

Where, ω^* is the given speed, ω_r is the reference trajectory of the speed which is the expected following value of the actual system after the softening treatment according to the expected trajectory. The softness factor $\alpha_r^i=e^{(-T_S/T_r)}$. Where, T_r is the expected system response time.

E. Receding Optimization

Receding optimization is through the optimization of a performance index to determine a control action of the future. Performance indicators are generally taken as the minimum variance between the object output at a certain time in the future and the desired trajectory at this moment. The quadratic performance index set of the cost function for the PMSM speed control is expressed as:

$$\min\Im=\sum_{i=1}^{h}[\omega_r(k+i)-\omega_m(k+i)-e(k+i)]^2+r^2 i_q^{*2}(k) \tag{14}$$

The equation can be written in another form of norm:

$$\Im = \| W_r(k) - W_m(k) - E(k) \|^2 \, Q_q + R_r i_q^{*2}(k) \quad (15)$$

Where: $W_r(k)_{(h\times 1)} = [\omega_r(k+1) \cdots \omega_r(k+h)]^T$

$$E(k)_{(h\times 1)} = [e(k+1) \cdots e(k+h)]^T$$

$Q_q(k)_{(h\times h)} = diag[q_1^2, \cdots, q_h^2]$ is the weighted coefficient of the controlled variables, and $R_{r(1\times 1)} = [r^2]$ is weighted coefficient of the input. Since the mechanical model of the motor is a linear characteristic, it can determine the minimum value of the cost function $\Im$ and the real-time update coefficient matrix at each sampling time. Let $\partial \Im / \partial i_q^* = 0$, and the controlled variable of i_q^* can be obtained.

$$\begin{aligned} i_q^* = (W_b^T Q_q W_b + R_r)^{-1} W_b^T Q_q [W_r(k) - W_o(k) \\ - E(k) - W_b \hat{T}_L(k) / K_t] \end{aligned} \quad (16)$$

Substituting the matrix data into (14) can be described as:

$$\begin{aligned} i_q^* = \{ & K_m q_1^2 [\omega_r(k+1) - \alpha_m \omega_m(k) - e(k+1) - K_m \hat{T}_L(k) / K_t] \\ & + K_m (1+\alpha_m) q_2^2 [\omega_r(k+2) - \alpha_m^2 \omega_m(k) - e(k+2) - \\ & K_m (1+\alpha_m) \hat{T}_L(k) / K_t] + \cdots + K_m (1+\alpha_m^{h-1}) q_h^2 [\omega_r(k+h) \\ & - \alpha_m^h \omega_m(k) - e(k+h) - K_m (1+\alpha_m^{h-1}) \hat{T}_L(k) / K_t \} / \{ K_m^2 [q_1^2 \\ & + (1+\alpha_m)^2 q_2^2 + \cdots + (1+\alpha_m + \cdots + \alpha_m^{h-1})^2 q_h^2] + r^2 \} \end{aligned} \quad (17)$$

According to the predictive function control algorithm, when combined with the vector control strategy of the PMSM servo system, the AC servo system with the PFC-PI cascade control is designed, using the PFC controller to replace the traditional automatic speed regulator. The block diagram of the simplified PMSM control system is shown in Fig. 2.

IV. PFC Design Using a Kalman Filter

The PFC controller lacks an external disturbance compensation term in the process of modeling, resulting in a degradation of the control performance in the dynamic processes of addition and subtraction of loads [12]. Servo systems usually adopt a photoelectric encoder to feedback the rotor position of the motor. Due to limited precision, speed direct differential acquisition is influenced by quantization errors and sampling noise.

With a low pass filter added after the speed measurement, a certain phase delay will be brought to affect the system's dynamic response. A Kalman filter has a better effect in terms of eliminating the system noise and measurement noise, at the same time it can estimate the related state and some of the parameters [18]. Therefore, the Kalman filter is designed to observe the load torque $\hat{T}_L$ and the rotor angular velocity $\hat{\omega}$. It then feeds them to the PFC controller. This can reconstruct the predictive function model and implement

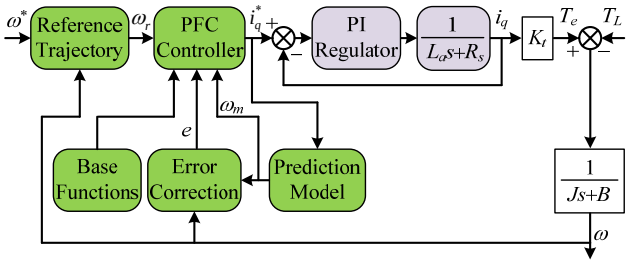

Fig. 2. Block diagram of the simplified PMSM control system using PFC method.

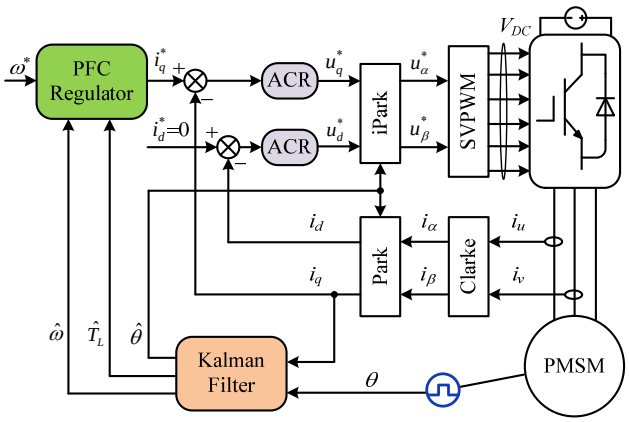

Fig. 3. Block diagram of the PMSM servo system with PFC and Kalman filter.

improvement over the original PFC controller, which improves the robustness against disturbances. The block diagram of the PMSM servo system with PFC and a Kalman filter is shown in Fig. 3.

According to the mechanical equation of the PMSM, the disturbance torque is extended to a state variable. The load torque cannot be derived from the formula. However, the changing rate of the load torque controller is much lower than sampling frequency, so it can be hypothesized that $dT_L/dt = 0$. Here, the basic form of state equation can be constructed as follows:

$$\begin{cases} dx/dt = Ax + Cu \\ y = Dx \end{cases} \quad (18)$$

Where, $x = (\omega \quad \theta \quad T_L)^T$, $u = T_e$, $y = \theta$,

$$A = \begin{bmatrix} -B/J & 0 & -1/J \\ 1 & 0 & 0 \\ 0 & 0 & 0 \end{bmatrix}, C = \begin{bmatrix} 1/J \\ 0 \\ 0 \end{bmatrix}, D = \begin{bmatrix} 0 \\ 1 \\ 0 \end{bmatrix}^T$$

In addition, the state variable x is the estimated value, the input variables u is the electromagnetic torque, and the output variable y is the rotor mechanical angular. In actual motor drive systems, it does need to use a discrete form in the digital system state equation. Meanwhile, there are all kinds of noise introduced by the existence of mathematical model parameter uncertainty and variability, and the quantization errors generated by the discretization and measurement errors. Bringing these uncertain factors into the system as a noise

vector w and a measurement noise vector v, can obtain the discretization form by formula (18) [20], as follows:

$$\begin{cases} x_{k+1} = A_k x_k + C_k u_k + w_k \\ y_k = D_k x_k + v_k \end{cases} \tag{19}$$

Where, x_k, y_k and u_k are the corresponding discrete forms of the state vector, output vector and input vector; w_k is the system noise; v_k is the measurement noise; and A_k, B_k and C_k are the discretization form of the system matrix, input matrix and output matrix. By the first-order approximate power series expansion, it is given by:

$$A_k = e^{AT} \approx I + AT_{KF} = \begin{bmatrix} 1 - BT_{KF}/J & 0 & -T_{KF}/J \\ T_{KF} & 1 & 0 \\ 0 & 0 & 1 \end{bmatrix} \tag{20}$$

$$C_k = \int_0^{T_{KF}} A^{e\tau} C d\tau \approx CT_{KF} = [T_{KF}/J \quad 0 \quad 0]^T \tag{21}$$

$$D_k = D = [0 \quad 1 \quad 0] \tag{22}$$

Where, T_{KF} is the sampling period of the Kalman filter. After discretization, the state vector and input variables can be represented as:

$$\hat{x}_k = [\hat{\omega}_k \quad \hat{\theta}_k \quad \hat{T}_{L_k}]^T, \; u_k = T_{e_k} \tag{23}$$

In order to estimate the disturbance item w_k of the discrete system, equation (19) can be rewritten as:

$$x_{k+1} = A_k x_k + C_k u_k + \Gamma \hat{w}_k \tag{24}$$

Where, $\hat{w}_k$ is the estimation of the disturbance term, and Γ is disturbance coefficient matrix. The disturbance of the system can be reflected by the deviation between the true and estimated values.

In order to carry on the estimation, the disturbance observer of discrete can be constructed as:

$$\begin{cases} \hat{w}_k = \Phi(z) w_{eq}(x, k-1) \\ w_{eq}(x, k-1) = \Gamma^+ (x_k - A_k x_{k-1} - C_k u_{k-1}) \end{cases} \tag{25}$$

Where, $w_{eq}(x, k-1)$ is the disturbance term associated with the discrete model, $\Gamma^+ = (C_k{}^T C_k)^{-1} C_k{}^T$ is left inverse matrix of the disturbance coefficient matrix, $\Phi(z) = H(zI - F)^{-1} G$ is a low pass filter to remove the high frequency harmonics of equation (19); F, G and H are the constant coefficient matrix. The Kalman filtering algorithm can be divided into a prediction section and a correction section, as shown in Table I.

Where, $\hat{w}_{k-1}$ is the observation value of the disturbance observer, $\hat{x}_{k|k-1}$ is the state prediction, P_k is the estimation error covariance matrix, $P_k = Cov(e_k) = E(e_k e_k^T) = \sum_{i=1}^{n} E\left[(x_i - \hat{x}_i)(x_i - \hat{x}_i)^T \right]$, $P_{k|k-1}$ is the priori error covariance matrix, $P_{k|k}$ is the posteriori error covariance matrix, K_k is the Kalman gain matrix, and I is the unit matrix. Combining the Kalman filtering algorithm and disturbance observer (25), the update recursive formula of the disturbance torque estimation is obtained as follows:

$$\hat{w}_k = F\hat{w}_{k-1} + G\Gamma_{k-1}^+ (x_{k|k} - A_{k-1}\hat{x}_{k-1|k-1} - C_{k-1}u_{k-1}) \tag{26}$$

The actual recursive calculation does not directly use the system noise vector w and measurement noise vector v. However, it uses the covariance matrix Q and R:

$$Q = Cov(w_k) = E(w_k w_k^T) \tag{27}$$

$$R = Cov(v_k) = E(v_k v_k^T) \tag{28}$$

The response errors in actual use do not influence each other. Therefore, let Q and R be as diagonal matrix so that $Q = diag[Q_\omega \quad Q_\theta \quad Q_{T_L}]$ and $R = [R_\theta]$. Where, Q_ω is the covariance of the angular velocity, Q_θ is the covariance of the angular displacement, Q_{T_L} is the covariance of the equivalent load, and R_θ is the covariance of the measurement error of the angular displacement. The value of the element in the system error covariance matrix Q depends on uncertainty, variability of the system model parameters and the quantization error of the continuity equation discretization. The value of the elements in the measurement error covariance matrix R depends on the quantization error of the A/D conversion, encoder accuracy and simulation of the noise intensity in the current sampling process. The state variable estimation error covariance matrix P has a small effect on the system steady state and dynamic process, and it has a certain influence on speed fluctuations when its value changes.

Under the condition of limited encoder accuracy, a Kalman filter is used to accurately observe the load torque, rotor

TABLE I
KALMAN FILTER ALGORITHM

Section	Algorithm
Predict section	$\hat{x}_{k\|k-1} = A_{k-1}\hat{x}_{k-1\|k-1} + C_{k-1}u_{k-1} + \Gamma_{k-1}^+ \hat{w}_{k-1}$
	$P_{k\|k-1} = A_{k-1}P_{k-1\|k-1}A_{k-1}^T + Q$
Verify section	$K_k = P_{k\|k-1}D_k^T (D_k P_{k\|k-1} D_k^T + R)^{-1}$
	$\hat{x}_{k\|k} = \hat{x}_{k\|k-1} + K_k (y_k - D_k \hat{x}_{k\|k-1})$
	$P_{k\|k} = (I - K_k D_k) P_{k\|k-1}$

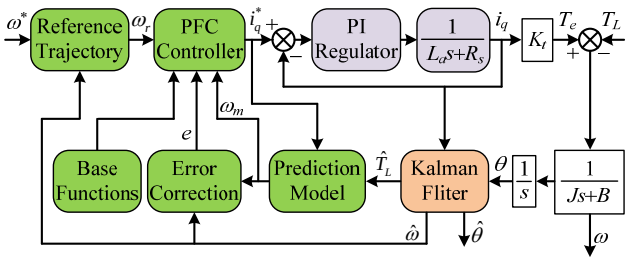

Fig. 4. Block diagram of the simplified PMSM control system using PFC method and Kalman filter.

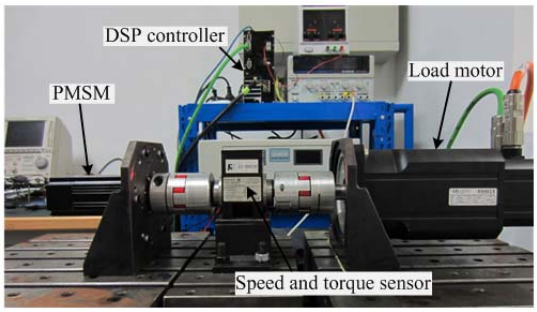

Fig. 5. Experimental test platform.

position and speed information, and the observation information is used for the PFC controller. It is used to construct a block diagram of a simplified PMSM servo system using the PFC method and a Kalman filter, as shown in Fig. 4.

V. Experimental Results and Analysis

To evaluate the system performance of the proposed improved PFC method with a Kalman filter for PMSMs, an experiment platform of a servo driving system has been built. It takes Infineon's XMC4500 chip based on the ARM® Cortex as the core, with a CPU frequency of 120 MHz. The control algorithms use SVPWM. As shown in Fig. 5, it mainly includes two parts, the measured servo system and the load system. The motor parameters of the measured servo system are shown in Table II. The servo system is driven by a three-phase pulse width modulation (PWM) inverter with an intelligent power module with a switching frequency of 10 kHz. The phase currents are measured by Hall-effect devices. The rotor position detection component uses an incremental photoelectric encoder of 2500 lines. The load motor and its controller choose Servo One industrial servo products of LUST, where the rated power of the motor is 3kW. The rotor position sensor uses a 24-bit multi ring absolute encoder from HEIDENHAIN.

The experimental results and analysis for the PI controller, PFC controller and PFC controller + Kalman filter (KF) are illustrated in Figs. 6–15 and TABLE III for five different scenarios: the tracking performance evaluation of the Kalman filter, observe torque performance evaluation, performance testing under electrical parameter uncertainties, trajectory tracking performance evaluation under several speeds, and performance testing during an abrupt change of the load torque. These are referred to as *A*, *B*, *C*, *D* and *E* in the following subsections.

A. Tracking Performance Evaluation of the Kalman Filter

To ensure accurate operation of the filter, it is necessary to determine the initial values of the covariance matrix *Q*, *R* and *P*. The selecting principle guarantees the steady state tracking and ensures that the filter does not suffer from divergence. The most commonly used method is trial and error method.

TABLE II
Parameters of the PMSM

Parameters	Value
Rated power (W)	400
Rated current (A)	1.9
Rated speed (rpm)	3000
Stator resistance (Ω)	5.8
Rated torque (N·m)	1.27
D-axis and Q-axis inductances (H)	0.0379
Number of pole pairs	4
Rotor flux (Wb)	0.3675
Moment of inertia (kg·m^2)	0.032×10^{-3}
Coefficient of friction (N·m·s /rad)	0.128×10^{-3}

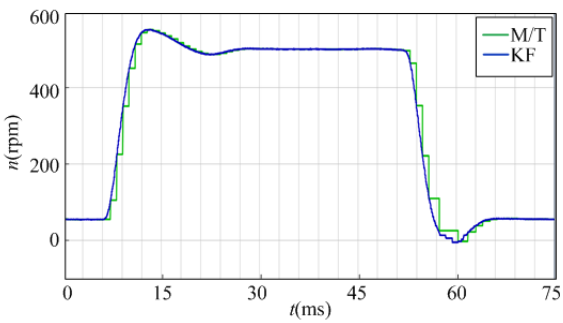

Fig. 6. Experimental response curves of the speed trajectory tracking for both M/T and Kalman filter (KF) method.

Multiple simulations and experiments are used to select the optimal performance of the initial values. The Kalman filter sampling time is 0.1 ms. The initial values are Q =diag[1, 0.06, 100], P = diag[0.1, 0.1, 0.1], and R=[0.5].

Fig. 6 shows a comparison of the experimental results between the observation speed with a Kalman filter (KF) and the M/T method to measure the speed. Given a speed change from 50rpm→500rpm→50rpm, the total sampling time is 75ms, the single computing time set to be 1ms and all of the sampling points are 4096. The M/T method and KF method can both detected the current speed well with a stable speed. However, when the speed changes, the M/T method has large delay and quantization fluctuations. Therefore, it cannot follow the speed change accurately. Meanwhile the observation results of the Kalman filter are stationary and almost without delay. Therefore, the observed speed can be used for the PFC control strategy.

B. Observe Torque Performance Evaluation of the Kalman Filter

In order to verify the performance of the Kalman filter to observe torque, an experimental comparison with the traditional DOB is carried out, as shown in Fig. 7. The observer gain is set to g=300 and the detection period is set to 0.5μs. A load of 0.5N·m was suddenly added at a speed of 300rpm. From Fig. 7(a), it can be seen that the observation results of the traditional disturbance observer-based (DOB) converged to a stable value within 0.3s and have a certain

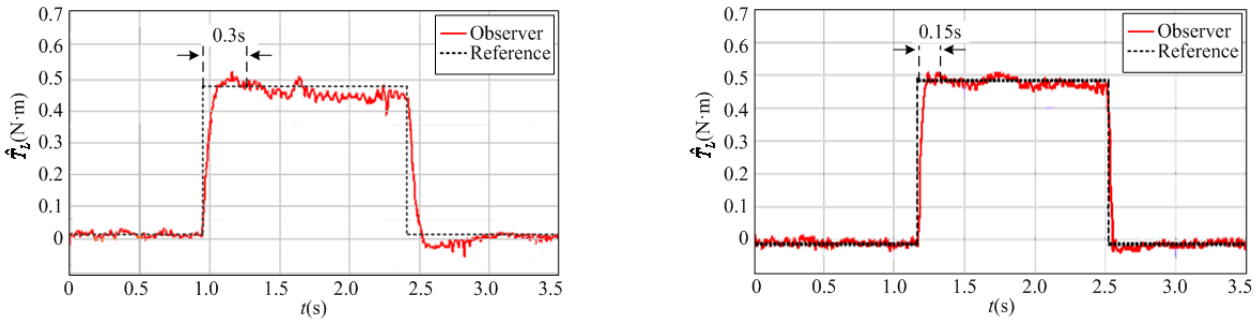

Fig. 7. Experimental response curves of the torque observer (a) DOB. (b) Kalman filter.

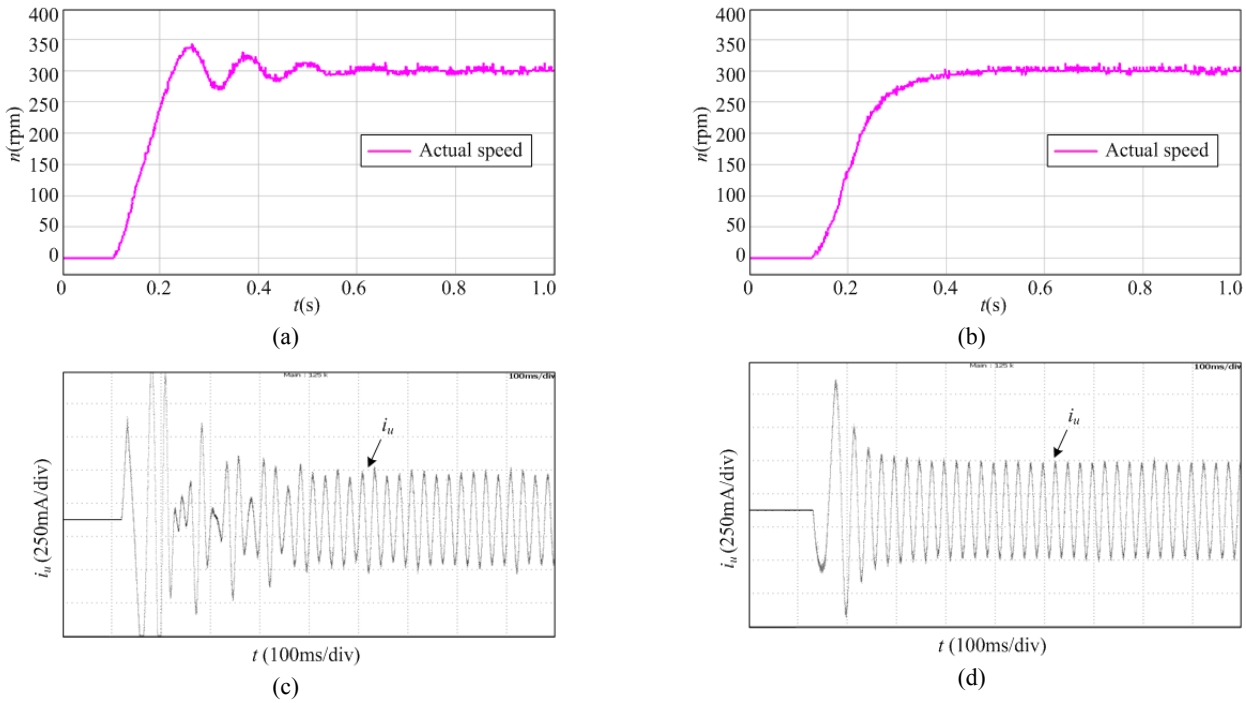

Fig. 8. Experimental response curves under uncertainty in the electrical parameters. (a) speed (PI). (b) speed (PFC+ KF). (c) i_u (PI). (d) i_u (PFC+KF).

overshoot. Fig. 7(b) shows the observed load torque with the Kalman filter. In a sudden load change, the Kalman observer can converge to a stable value within 0.15s and it has a small overshoot, which is better than the traditional DOB.

C. Uncertainty in the Electrical Parameters

To verify the robustness of a PMSM servo system using the proposed PFC + Kalman filter control scheme, the armature resistance, stator inductance and rotor-flux linkage, were set incorrectly in the controller. In comparison with the real values, the value of these three electrical parameters were respectively increased by 35%, decreased by 35% and decreased by 25%. As shown in Fig. 8(a), the motor speed has developed a big overshoot under the PI controller, and in Fig. 8(b) the motor speed can be seen to converge to 300rpm under the presented control scheme. Fig. 8(c) and Fig. 8(d) show the phase current waveforms. Comparing the variation of the two curves, it can be seen that the latter has less sensitivity to the mismatched mechanical parameters than the former.

D. Speed Trajectory Tracking Performance Evaluation

The speed trajectory tracking performance is investigated under three control methods. Figs. 9-12 shows the speed response waveforms under several given values, they are 3 rpm, 300 rpm, 1500 rpm and 3000 rpm. Then the no-load speed response was detected respectively in the PI controller, PFC controller, and PFC controller + Kalman filter. The parameters for the PI speed controller are: $K_p = 8.5$, $K_i = 1$; for the PI regulators of both current loops they are: $K_p = 39$, $K_i = 2400$; for the PFC controller they are: $\alpha_m = 0.9548$, $\alpha_r = 0.0183$, $K_m = 1550$; for the PFC control sampling period $T_s = 0.5$ ms; and for the reference trajectory expected

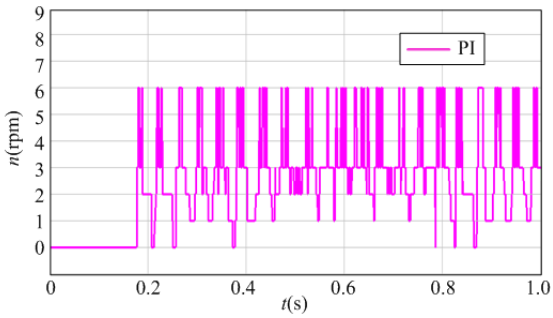

(a)

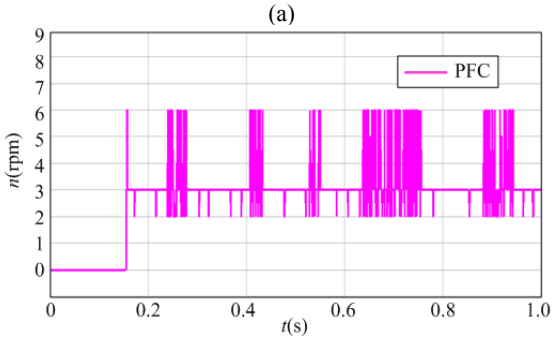

(b)

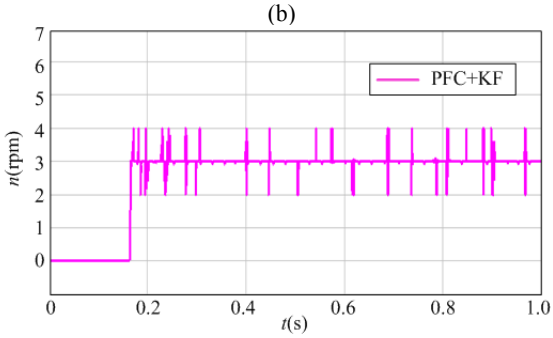

(c)

Fig. 9. Experimental response curves in case of 3 rpm speed trajectory tracking. (a) PI controller. (b) PFC controller. (c) PFC controller +Kalman filter (KF).

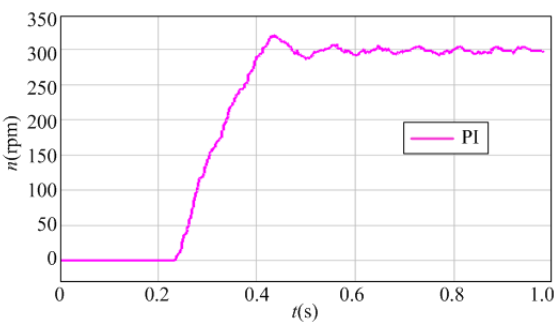

(a)

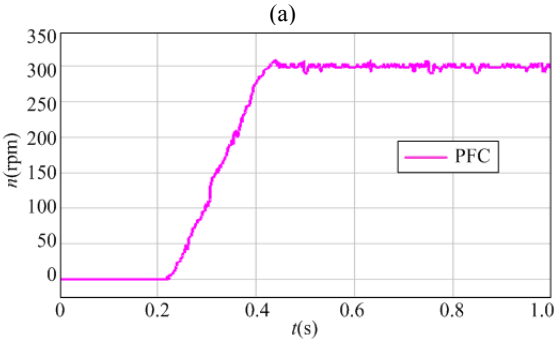

(b)

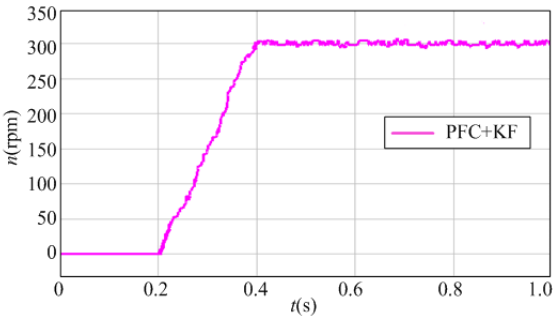

(c)

Fig. 10. Experimental response curves in case of 300 rpm speed trajectory tracking. (a) PI controller. (b) PFC controller. (c) PFC controller +Kalman filter (KF).

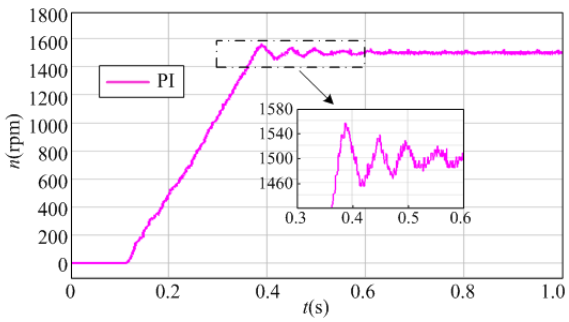

(a)

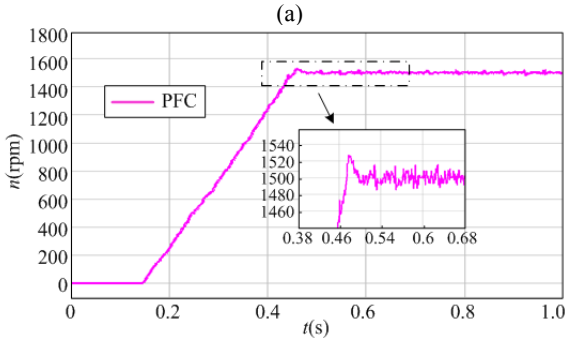

(b)

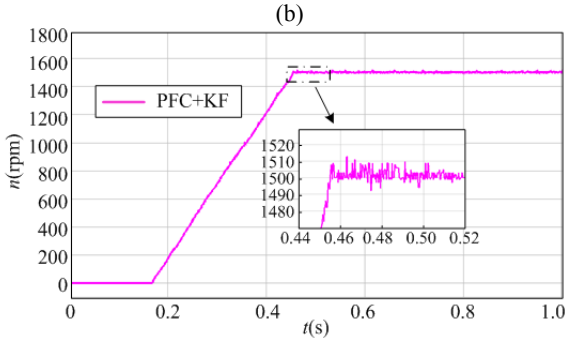

(c)

Fig. 11. Experimental response curves in case of 1500 rpm speed trajectory tracking. (a) PI controller. (b) PFC controller. (c) PFC controller +Kalman filter (KF).

closed-loop time $T_r = 0.05$ ms.

The performance indexes of the three control methods under different conditions are shown in TABLE III, where, OS is the overshoot, t_p is the peak time, t_s is the setting time, the tolerance band of t_s is selected as ±2%, and K_{fn}

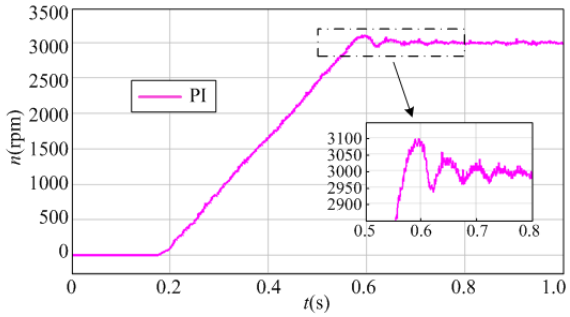

(a)

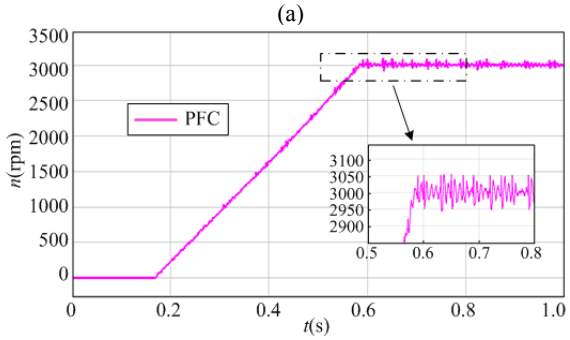

(b)

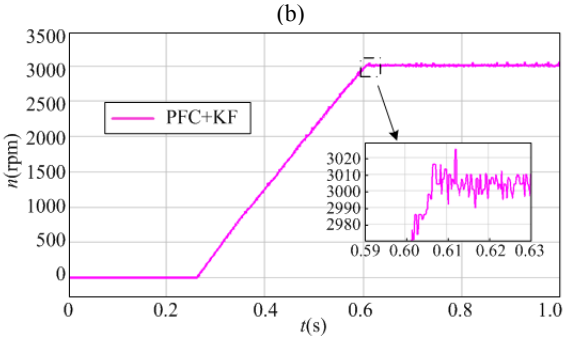

(c)

Fig. 12. Experimental response curves in case of 3000 rpm speed trajectory tracking. (a) PI controller. (b) PFC controller. (c) PFC controller + Kalman filter (KF).

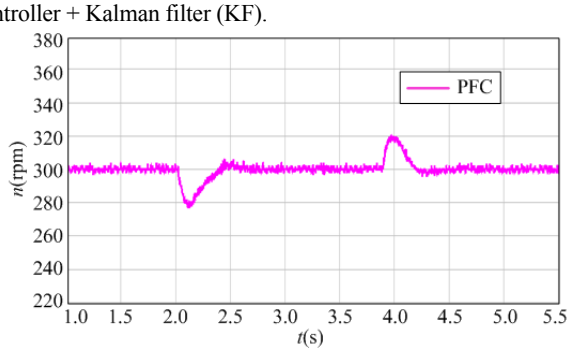

(a)

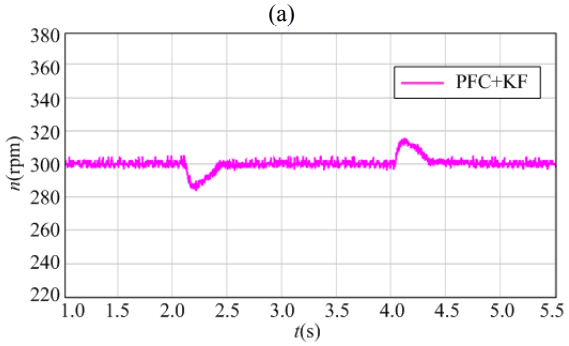

(b)

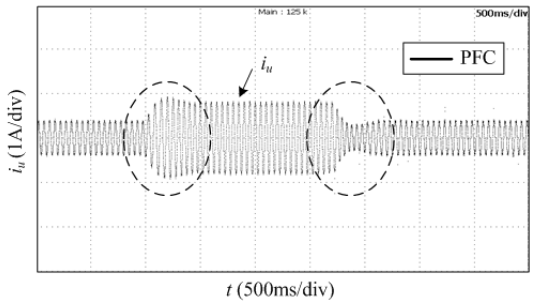

(c)

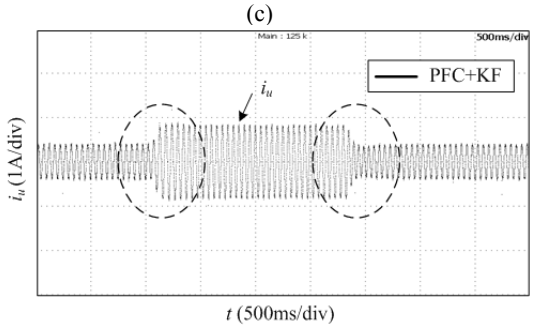

(d)

Fig. 13. Experimental response curves in case of 300 rpm speed trajectory tracking under a sudden load torque disturbance. (a) speed (PFC). (b) speed (PFC+ KF). (c) i_u (PFC). (d) i_u (PFC+KF).

TABLE III
COMPARISON OF PERFORMANCE INDICES

Reference Speed	Indices	Control Scheme		
		PI	PFC	PFC+KF
3(rpm)	OS(%)	100	100	33.3
	t_p(ms)	7.6	7.4	11.5
	K_{fn}(%)	71.4	50.0	33.3
300(rpm)	OS(%)	7.5	3.3	1.8
	t_s(ms)	276	223	201
	K_{fn}(%)	3.6	2.7	1.7
1500(rpm)	OS(%)	3.7	1.8	0.9
	t_s(ms)	361	297	272
	K_{fn}(%)	0.53	0.49	0.41
3000(rpm)	OS(%)	3.2	1.7	0.8
	t_s(ms)	446	401	335
	K_{fn}(%)	0.83	1.56	0.38

is the steady speed ripple coefficient, $K_{fn} = \frac{n_{max} - n_{min}}{n_{max} + n_{min}} \times 100\%$.

Compared with other two controllers, the experimental results show that the proposed control system has better performance in both the dynamic and steady states. It shows the smallest overshoot, the shortest settling time and the least steady speed ripple.

E. Performance Evaluation under an Abrupt Change of the Load Torque

This test was performed to verify the performance of the proposed control strategy in terms of its disturbance rejection capability. Figs. 13-15 show the speed and phase current

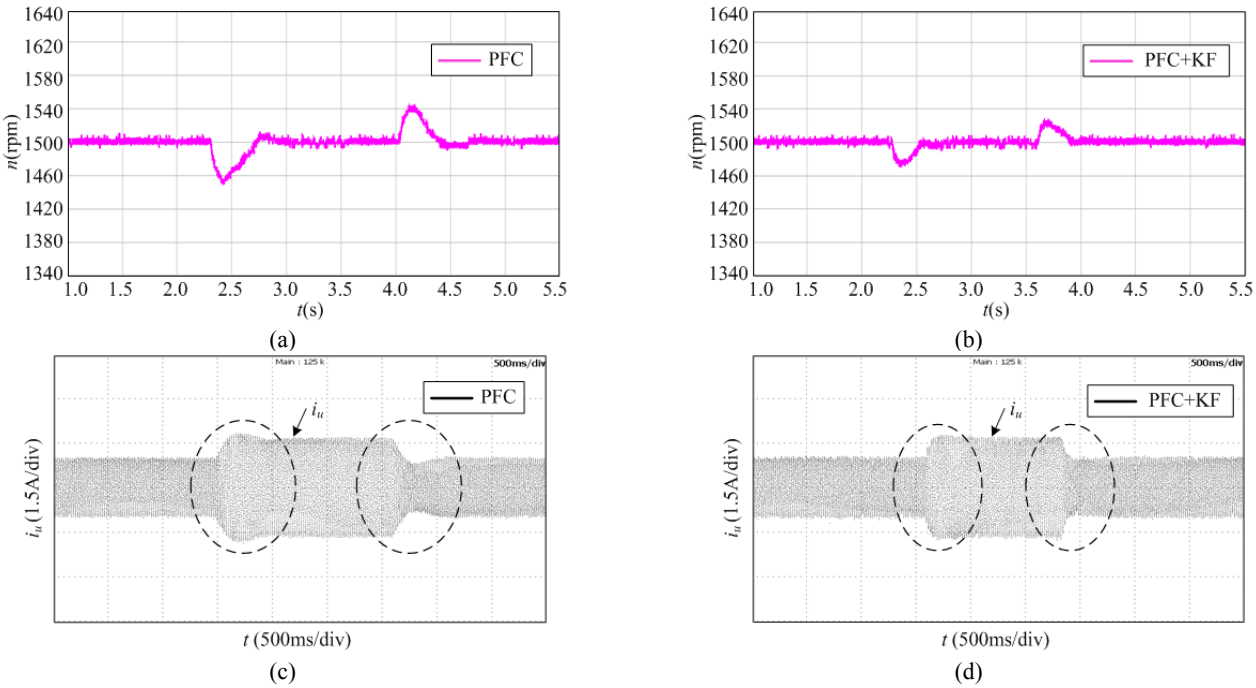

Fig. 14. Experimental response curves in case of 1500 rpm speed trajectory tracking under a sudden load torque disturbance. (a) speed (PFC). (b) speed (PFC+ KF). (c) i_u (PFC). (d) i_u (PFC+KF).

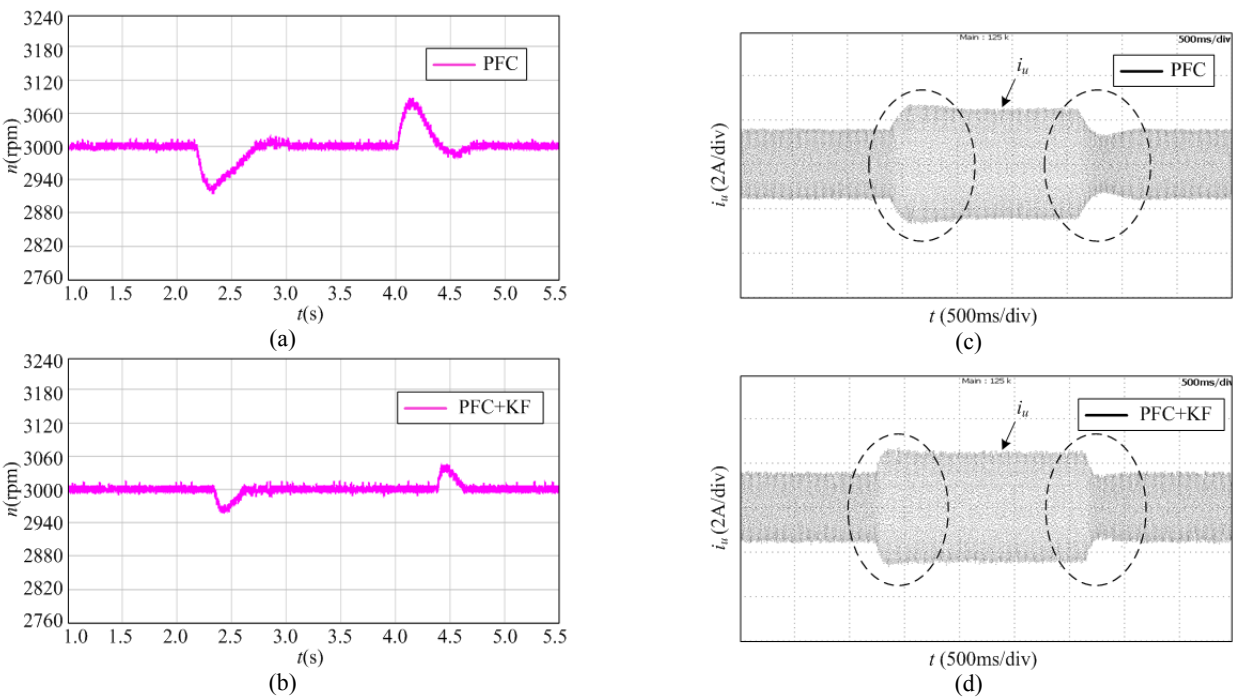

Fig. 15. Experimental response curves in case of 3000 rpm speed trajectory tracking under a sudden load torque disturbance. (a) speed (PFC). (b) speed (PFC+ KF). (c) i_u (PFC). (d) i_u (PFC+KF).

response waveforms under three given values, they are 300rpm, 1500rpm and 3000rpm. The results are shown in Figs. 13-15 when adding an abrupt pulse shape 0.5N·m load. Compared with the PFC method, the proposed PFC + Kalman filter method has a less of a speed decrease and a shorter recovery time while maintaining a good dynamic performance. In addition, the steady-state error is quickly removed, while the phase current has a faster response and a smaller current fluctuation.

VI. CONCLUSION

The quantization error of low resolution encoders, sampling noise and external torque disturbances affect the

precision of PFC prediction models in servo systems. This in turn degrades the whole system dynamic performance. This paper presents an improved PFC control strategy with a Kalman filter, using the speed information and load torque observed by the Kalman filter to reconstruct the PFC model. This method can raise the model accuracy and it improves standard PFC systems. The experimental results show that the proposed control strategy can effectively suppress the quantization error of velocity measurements and sampling noise influence. It can also enhance the system dynamic control performance and disturbance rejection.

ACKNOWLEDGMENT

The authors would like to thank the support from National 863 Project of China High-Tech Development Plan (Project No. 2011AA04A105).

REFERENCES

[1] C. Line, C. Manzie, and M. C. Good, "Electromechanical brake modeling and control: From PI to MPC," *IEEE Trans. Control Syst. Technol*, Vol. 16, No. 3, pp.446-457, May 2008.

[2] X. D. Li and S. H. Li. "Speed control for a PMSM servo system using model reference adaptive control and an extended state observer," *Journal of Power Electronics*, Vol. 14, No. 3, pp. 549-563, May 2014.

[3] R. Errouissi, M. Ouhrouche, W. H. Chen, and A. M. Trzynadlowski, "Robust nonlinear predictive controller for permanent-magnet synchronous motors with an optimized cost function," *IEEE Trans. Ind. Electron*., Vol. 59, No. 7, pp. 2849-2858, Jul. 2012.

[4] J. W. Jung, H. H. Choi, and T.-H. Kim "Fuzzy PD speed controller for permanent magnet synchronous motors," *Journal of Power Electronics*, Vol.11, No. 6, pp. 819-823, Nov. 2011.

[5] F. J. Lin, T. S. Lee, and C.-H. Lin, "Robust H_∞ controller design with recurrent neural network for linear synchronous motor drive," *IEEE Trans. Ind. Electron*., Vol. 50, No. 3, pp. 456-470, Jun. 2003.

[6] N. Z. Jin, X. D. Wang, and X. G Wu, "Current sliding mode control with a load sliding mode observer for permanent magnet synchronous machines," *Journal of Power Electronics*, Vol. 14, No. 1, pp. 105-114, Jan. 2014.

[7] T. Satoh, K. Kaneko, and N. Saito, "Performance improvement of predictive functional control: a disturbance observer approach," *IEEE 37th Annual Conference on Ind. Electronics Society,* pp. 669-674, 2011.

[8] M. Preindl and E. Schaltz, "Sensorless model predictive direct current control using novel second-order PLL observer for PMSM drive systems," *IEEE Trans. Ind. Electron*., Vol. 58, No. 9, pp. 4087-4095, Sep. 2011.

[9] J. S. Ko and J. S. Choi, "Maximum torque control of an IPMSM drive using an adaptive learning fuzzy-neural network," *Journal of Power Electronics*, Vol. 12, No. 3, pp. 819-823, May 2012.

[10] F. M. Fayez, "Robust recurrent wavelet interval type-2 fuzzy-neural-network control for DSP-based PMSM servo drive systems," *Journal of Power Electronics*, Vol. 13, No. 1, pp. 139-160, Jan. 2013.

[11] F. Morel, X. F. ShiLin, J. M. Retif, B. Allard, and C. Buttay, "A comparative study of predictive current control schemes for a permanent magnet synchronous machine drive," *IEEE Trans. Ind. Electron*., Vol. 56, No. 7, pp. 2715-2728, Jul. 2009.

[12] R. Errouissi, M. Ouhrouche, W. H. Chen, and A. M. Trzynadlowski, "Robust cascaded nonlinear predictive control of a PMSM with anti-windup compensator," *IEEE Trans. Ind. Electron*., Vol. 59, No. 8, pp. 3078-3088, Aug. 2012.

[13] S. Chai, L. P. Wang, and E. Rogers, "A cascade MPC control structure for a PMSM with speed ripple minimization," *IEEE Trans. Ind. Electron*., Vol. 60, No. 8, pp. 2978-2987, Aug. 2013.

[14] J. Richalet, "Industrial applications of model based predictive control," *Automatica*, Vol. 29, No. 5, pp. 1251-1274, Sep. 1993.

[15] M. Preindl and S. Bolognani, "Model predictive direct speed control with finite control set of PMSM drive systems," *IEEE Trans. Power. Electron*., Vol. 28, No. 2, pp. 1007- 1015, Feb. 2013.

[16] H. X. Liu and S. H. Li. "Speed control for PMSM servo system using predictive functional control and extended state observe," *IEEE Trans. Ind. Electron*., Vol. 59, No. 2, pp. 1171-1183, Feb. 2012.

[17] W. H. Ali, M. Gowda, P. Cofie, and J. Fuller, "Design of a speed controller using extended Kalman filter for PMSM," *IEEE 57th International Midwest Symposium on Circuits and Systems*, pp. 1101-1104, 2014.

[18] Z. G. Yin, R. F. Zhang, Z. Yanru, and C. Yu, "Speed and flux estimation of permanent magnet synchronous motor for sensorless vector control based on robust extended Kalman filter," *IEEE International Symposium on Ind. Electronics*, pp. 748-751, 2012.

[19] N. K. Quang, N. T. Hieu, and Q. P. Ha, "FPGA-based sensorless PMSM speed control using reduced-order extended Kalman filters," *IEEE Trans. Ind. Electron*., Vol. 61, No. 12, pp. 6574-6582, Dec. 2014.

[20] Z. D. Zheng and Y. D. Li, "Load torque observer of permanent magnet synchronous motor," *Transactions of China Electrotechnical Society*, Vol. 25, No. 2, pp. 30-36, Feb. 2010.

[21] X. Xiao and C. M. Chen, "Reduction of torque ripple due to demagnetization in PMSM using current compensation," *IEEE Trans. Appl. superconduct*., Vol. 20, No. 3, pp. 1068 -1071, Jun. 2010.

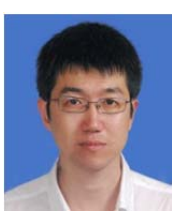

Shuang Wang was born in Jilin, China, in 1977. He received his B.S., M.S. and Ph.D. degrees in Electrical Engineering from Harbin Institute of Technology, Harbin, China, in 2000, 2005 and 2009, respectively. Since 2010, he has been with the School of Mechatronic Engineering and Automation, Shanghai University, Shanghai, China, where he is presently working as Assistant Professor. His current research interests include intelligent control theory and its application to new energy vehicles, power electronics and servo control systems.

Wenju Zhu was born in Tangshan, China, in 1986. He received his B.S. degree in Electrical Engineering from Shanghai Dianji University, Shanghai, China, in 2010. He is presently a postgraduate student at Shanghai University, Shanghai, China. He has been an Electrical Engineer in the Shanghai STEP Electric Co., Shanghai, China, from 2010 to 2013. His current research interests include new energy vehicles, control theory and its application to electric drive servo systems.

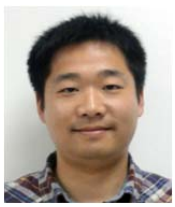

Jian Shi was born in Henan, China, in 1982. He received his M.S. degree in Electrical Engineering from Fuzhou University, Fuzhou, China, in 2007, and his Ph.D. degree in Electrical Engineering from Harbin Institute of Technology, Harbin, China, in 2013. From 2007 to 2010, he worked for the ThyssenKrupp Elevator Co., China as a Research Engineer. Since 2014, he has been a post-doctoral researcher in Shanghai University, Shanghai, China. His current research interests include electric machines, power electronics and control systems.

Hua Ji was born in Qingdao, China, in 1977. She received her M.S. degree in Electrical Engineering from Nanjing University of Aeronautics and Astronautics, Nanjing, China, in 2004. Since 2004, she has been with the Department of Electrical and Electronic Engineering, Shandong University of Technology, Zibo, China, where she is presently an Associate Professor. Her current research interests include the study of high performance servo control systems.

Surong Huang was born in Shanghai, China. He received his Ph.D. degree from the Shanghai University of Technology, Shanghai, China, in 1977. In 1977, he joined the Shanghai University of Technology, where he was promoted to Associate Professor and then Professor, in 1993 and 2001, respectively. He was a Visiting Faculty Member in the Department of Electrical and Computer Engineering, University of Wisconsin, Madison, WI, USA, from 1995 to 1996 and from 1998 to 2000. He is currently a Professor and Doctoral Supervisor in the Department of Automation, Shanghai University, Shanghai, China. He is engaged in research and development on new types of electrical machines and drive systems. His current research interests include the design, control, modeling and simulation of electrical machines and ac drives, and the vibration and noise analysis of electrical machines. He has published more than 100 papers on these topics.